JOC The Journal of Organic Chemistry

Article

pubs.acs.org/joc

Atropisomers of Arylmaleimides: Stereodynamics and Absolute Configuration†

Martina Ambrogi,‡ Alessia Ciogli,§ Michele Mancinelli,‡ Silvia Ranieri,‡ and Andrea Mazzanti*,‡

‡Department of Industrial Chemistry "Toso Montanari", University of Bologna, Viale Risorgimento 4, 40136 - Bologna, Italy

§Dipartimento di Chimica e Tecnologie del farmaco, Università di Roma "La Sapienza", P.le A.Moro 5, 00185 - Roma, Italy

Supporting Information

ABSTRACT: 4-Aryl-3-bromo-*N*-benzylmaleimides and 3,4-biaryl-*N*-benzylmaleimides have been synthesized by a modified Suzuki cross-coupling reaction from 3,4-dibromo-*N*-benzylmaleimide. The conformational studies by dynamic NMR and DFT calculations showed that the interconversion barrier between the two available skewed conformations is under steric control. When the aryl group was a 2-methylnaphthyl, thermally stable atropisomers were isolated by enantioselective HPLC and their absolute configurations were assigned by TD-DFT simulations of the ECD spectra.

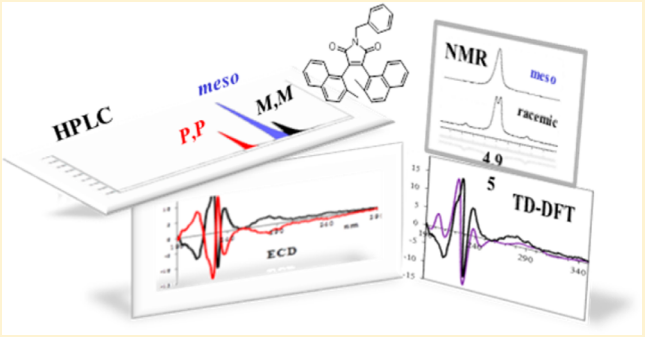

INTRODUCTION

Restricted rotation around bonds in molecules can result in the formation of atropoisomers.[1] Provided that the necessary geometric requirements are met, atropoisomers might be chiral and configurationally stable. The conformational properties of atropisomeric molecules have attracted interest in recent years due to their applications to drug discovery,[2] and the synthesis of enantiopure atropisomers of natural products is also an open research field.[3] Many effective organocatalysts are based on an atropisomeric scaffold such as BINOL,[4] and atropisomeric phosphines are well-known as chiral ligands in metal catalysis.[5] In the vast majority of cases, atropisomeric molecules have a planar framework with one or more substituents linked in key sites. These substituents, which are often variously decorated aromatic groups, adopt tilted conformations relative to the molecular plane, thus generating a stereogenic axis. Depending on the hindrance of the substituents and on the geometry of the planar framework, the resulting conformational enantiomers can be either stereolabile or configurationally stable (atropisomers[6]). The corresponding barriers of interconversion can be usually determined by means of variable-temperature NMR spectroscopy,[7] NMR kinetic methods (EXSY and standard kinetic measurements), dynamic HPLC, and GC.[8,9]

3,4-Disubstituted maleimides exhibit biological properties including antibacterial and antiviral activity, and they are potent inhibitors of glycogen synthase kinase-3 (GSK-3).[10] Substituted maleimides which have extended conjugation have been considered as light-emitting diodes (OLED)[11] and fluorescence devices.[12] Nelson et al.[13] found that a pair of indolyl substituents do not allow to obtain maleimidic atropisomers, and they were able to generate stable atropisomers only by constraining the two heterocyclic rings into a macrocycle. Based on previous experiences,[14] in the present work it was exploited the ability of the maleimide scaffold to generate stable atropisomers when two unsymmetrically substituted aryl rings are bound to the 3,4-position. Their separation by means of HPLC and the determination of the absolute configuration will be also pursued.

RESULTS AND DISCUSSION

To determine the steric requirements necessary to obtain stable atropisomers of bis-arylmaleimides and to keep a reactive site in the molecule (compounds **3**), a set of *o*-aryl-substituted boronic acids were reacted with 3,4-dibromobenzylmaleimide (see Scheme 1). Different synthetic approaches have been reported for the preparation of 3,4-disubstituted maleimides, most of which are based on metal-catalyzed cross-coupling reactions of 3,4-dihalomaleimides.[15] A modified Suzuki coupling, under milder conditions, was found to be the most effective approach to obtain the compounds reported in Scheme 1. Anhydrous conditions were required to preserve the imidic moiety when highly hindered boronic acids were used, and dry THF was used together with solid Cs_2CO_3 under inert atmosphere (see the Experimental Section).

Bis-aryl Maleimides. When equal aryl substituents, lacking a local C_2-symmetry axis, are bonded in appropriate positions to planar frameworks (such as benzene,[16] naphthalene,[17] phenanthrene,[18] anthracene,[19] acenaphthene,[20] acenaphthylene,[21] and biphenylene[22]), configurationally stable isomers or stereolabile *syn*/*anti* conformers are formed, depending on the extent of the steric hindrance. The existence of *syn*/*anti* stereoisomers is the

Received: January 29, 2013
Published: March 25, 2013

   dx.doi.org/10.1021/jo400200v | J. Org. Chem. 2013, 78, 3709−3719

Scheme 1. Preparation of Compounds 3a–f and 4a–f

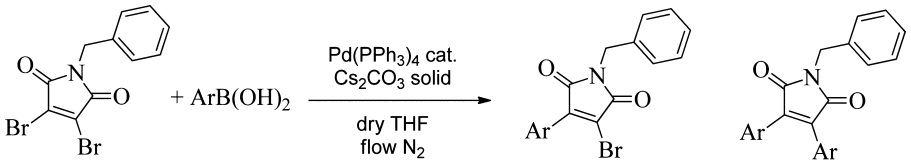

Ar = 2-methylphenyl (**a**), 2-ethylphenyl (**b**), 2,3-dimethylphenyl (**c**), 2-isopropylphenyl (**d**), 1-naphthyl (**e**), 2-methylnaphthyl (**f**).

consequence of the planes of the two aryl substituents being twisted with respect to the planar scaffold (see Scheme 2).

Scheme 2. Steric and π Barriers in Aryl–Aryl Compounds

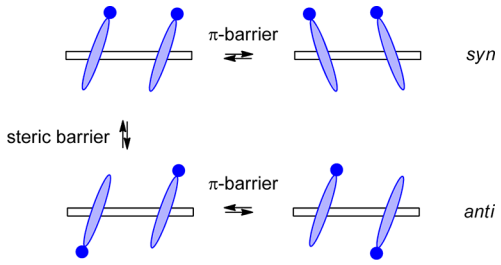

In these situations, the substituent on the aryl ring can stay either on the same (*syn*) or on the opposite side (*anti*) with respect to the other one. Their interconversion, corresponding to a 180° rotation, requires passage through a transition state where one ring is coplanar with the scaffold (Scheme 2, steric barrier[8]). It was also pointed out that the twisted disposition of the two aryl rings would allow the *syn* form to originate a pair of enantiomers that interconvert through a transition state where the rings are nearly orthogonal to the scaffold (Scheme 2, π-barrier[8]): this process corresponds to a torsion around the bond connecting the aryl group to the scaffold (also called flipping process) of approximately 90°. In the case of the *anti* form, on the other hand, this nearly 90° torsion would create two conformational diastereoisomers with different stability, identified as *anti*-in and *anti*-out.[9] Each of these conformers exists as a pair of enantiomers, but their enantiomerization requires the passage through the *syn* isomer, i.e., the 180° rotation involving the steric barrier (Scheme 2). However, the π-barrier is usually very low, and its value decreases with the increasing of the steric barrier. Indeed, this feature was observed by dynamic NMR only in one case on a meta-substituted bis-aryl biphenylene.[14a]

In the case of maleimides, DFT computational studies[23] support the existence of different *syn* and *anti* conformers due to the skewed disposition of the two aryl rings. However, the aryl rings are not perpendicular to the maleimide plane; thus, two diastereoisomeric conformations are available for the *anti* form, whereas the *syn* yields a fast-exchanging enantiomeric pair (see Scheme 3).

To theoretically analyze the stereodynamic pathways, we performed DFT optimization of both ground states and of the available transition states at the B3LYP/6-31G(d) level of theory (see Table 1). The calculated energy value for the π-barrier of the less hindered compound **4a** suggested a value as low as 3.8 kcal/mol; thus, for the following conformational analysis the *syn* and *anti* conformations can be considered as the average of the limiting structures.

When the *ortho* substituents of the aryl rings are both on the same side of the maleimide scaffold, and a fast interconversion due to π-barrier is taken into account, the conformation has an average C_s symmetry and corresponds to a *meso* form (*syn* in

Scheme 3. Stereodynamic Network of 3,4-Bisarylmaleimides[a]

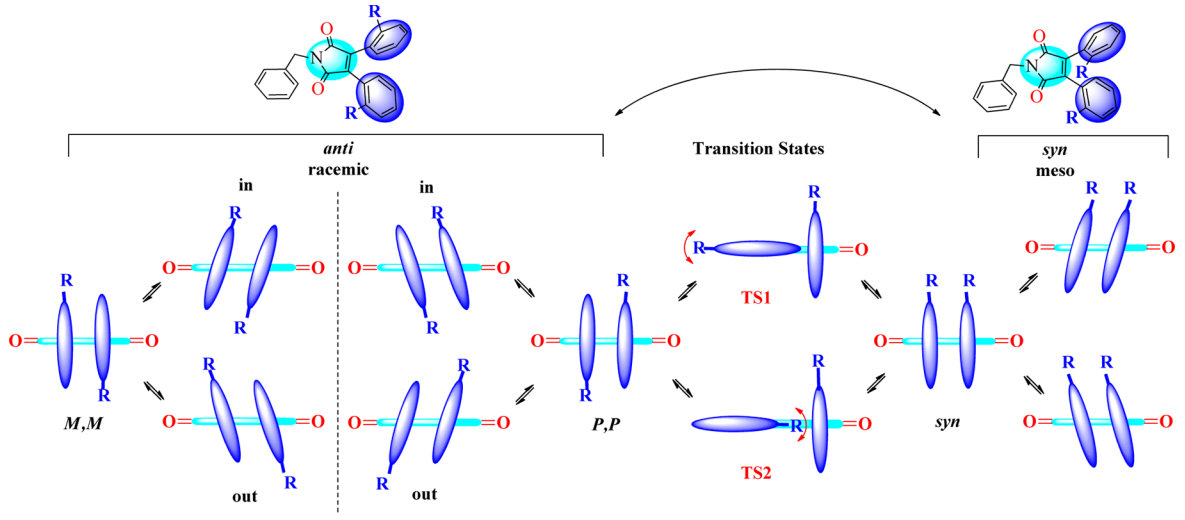

[a]Blue: aryl rings. Cyan: maleimide ring.

dx.doi.org/10.1021/jo400200v | J. Org. Chem. 2013, 78, 3709–3719

Table 1. DFT-Computed Energies of 3,4-Bisaryl-*N*-benzylmaleimides 4a–f[a]

entry	GS1 (*anti*-out)	GS2 (*anti*-in)	GS3 (*syn*)	TS1	TS2	expt $\Delta G^{\ddagger}$[b]	*syn*/*anti* ratio[c]
4a	0.00	0.67	0.28	11.55	12.44	12.9	55/45
4b	0.00	0.95	0.47	12.86	13.44	14.0	54/46
4c	0.00	0.58	0.16	13.93	14.61	14.9	55/45
4d	0.00	1.81	1.33	14.42	15.93	15.5	49/51
4e	0.39	0.00	0.00_1	12.88	13.00	14.0	45/55
4f	0.22[d]	0.48[d]	0.00	23.53	25.12	24.5	51/49

[a]The last two columns report experimental energy barriers ($\Delta G^{\ddagger}$ in kcal/mol) and experimental *syn*/*anti* ratios. [b]This value corresponds to the *syn*/*anti* interconversion, derived from line shape simulations. See text for more details. [c]Determined by NMR integration at appropriate temperature. [d]The assignment refers to the relative position of the 2-methyl groups.

Schemes 2 and 3). On the contrary, if the *ortho* substituents of the aryl groups are arranged on the opposite sides of maleimide (*anti* configuration), the resulting C_2 symmetry implies a pair of conformational enantiomers. The interconversion pathway between the *syn* and *anti* conformations can be completed through two transition states (TS1 and TS2 in Scheme 3). TS1 represents the crossing of the *o*-aryl substituent on the carbonyl group, while TS2 corresponds to the internal crossing of the *ortho*-substituent on the second aryl ring.[15a]

In order to experimentally detect these conformations, the hindrance caused by the *ortho* substituent on the aryl groups must generate an energy barrier of interconversion ($\Delta G^{\ddagger}$) within the dynamic NMR range (4.5–22 kcal/mol). When the interconversion barrier is frozen on the NMR time scale, two conformational diastereoisomers can be observed. However, the assignment of the two sets of signals to the *meso* or racemic form cannot be extracted by a simple NMR spectrum, and the use of a chirality probe is required. To avoid any steric interference with the two aryl groups, a benzyl group was bonded to the nitrogen of maleimide. The benzyl moiety was chosen for the presence of an uncoupled CH_2 group that acts as the chirality probe, thus displaying different multiplicity depending on the molecular symmetry.[24] The very fast rotation of the benzyl group guarantees that diastereoisomeric conformations due to different dispositions of the benzyl moiety cannot be observed in the actual temperature range (i.e., >−100 °C). The effect of the molecular symmetry on the NMR signal of the CH_2 is shown in Figure 1 for compound **4d** (Ar = 2-isopropylphenyl). The variable-temperature spectra of other compounds can be found in the Supporting Information (Figures S1–S9).

Because of the slow *syn*/*anti* interconversion rate between the two conformations, at room temperature the signal of the CH_2 is very broad and unresolved. At 0 °C, the process is slow on the NMR time scale and the signals of the *syn* and *anti* conformers are distinguishable. The singlet in the middle of the spectrum (4.826 ppm, cyan) corresponds to the *syn* conformation (C_s symmetry, 49%), whereas the AB system (red sections of the spectrum) corresponds to the *anti* conformation (C_2 symmetry, 51%). The line shape simulation must take into account the coupling constant of the AB spin system and the exchange of the AB lines with the singlet of the *syn* form. A second rate constant, corresponding to the racemization of the *anti* forms should be also considered.

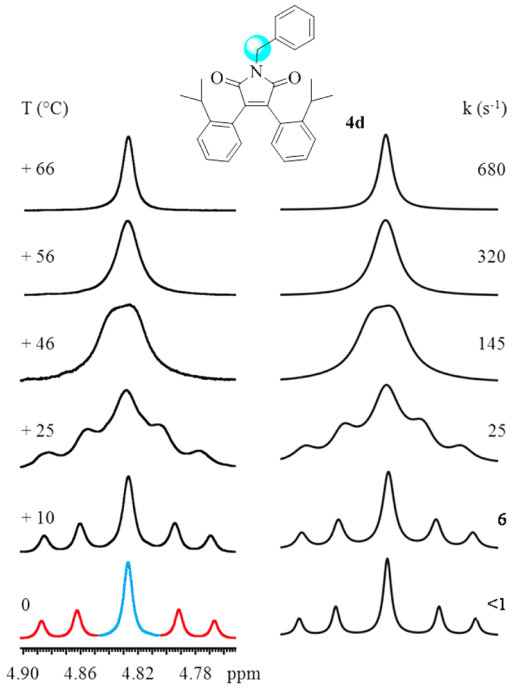

Figure 1. (Left) Temperature dependence of the ^{1}H benzylic CH_2 signal of **4d** (600 MHz in $C_2D_2Cl_4$). (Right) Line shape simulation obtained with the rate constants reported.

An accurate simulation was obtained by using only one rate constant which exchanged the AB system with the single signal of the *syn* form, without the direct exchange within the AB system. This means that the racemization of the *anti* conformer corresponds to a two-step mechanism with the *syn* conformation as an intermediate. The experimental free energy thus corresponds to the transition state of the *anti*-to-*syn* process, and not to the racemization of the conformational enantiomers. To determine this energy barrier, a 1/2 factor must be considered for the rate constants to account for the possibility of any of the two rings to generate the *syn* isomer by rotation. The experimental energy barrier obtained by line shape simulation for **4d** was 15.5 ± 0.1 kcal/mol, and the $\Delta G^{\ddagger}$ values were almost invariant with the temperature, thus implying that the activation entropy was very small or negligible. This situation is usually found in conformational processes where only an internal rearrangement takes place.[7] DFT calculations had suggested that the lower energy transition state was TS1 (calculated value: 14.4 kcal/mol). This value matches satisfactorily the experiment, the difference being only 1.1 kcal/mol (a summary of the experimental and calculated barriers is reported in Table 1). Although B3LYP does not consider dispersive forces,[25] and despite the use of a relatively small basis set prone to BSSE errors, this theoretical level confirmed to be able to reproduce with good accuracy the energy barriers of conformational processes.

The energy barriers obtained for compounds **4a–e** suggest that the barrier is controlled only by steric factors, and the computed energies matched well the relative stability of the two conformational diastereoisomers, as well as the energy barriers for their interconversion.

B3LYP calculations provided transition energies of 23.5 and 25.1 kcal/mol for the *syn*/*anti* interconversion in the case of compound **4f** (Ar = 2-methylnaphthyl), thus implying the presence of thermally stable atropisomeric forms. To our

dx.doi.org/10.1021/jo400200v | J. Org. Chem. 2013, 78, 3709–3719

delight, the theoretical predictions were validated by experimental results. The ^{1}H NMR spectrum of the crude product showed two sets of signals, supporting the existence of diastereoisomeric forms, at least on the NMR time scale. Even when the sample was heated to 120 °C in $C_2D_2Cl_4$, no evidence of a dynamic exchange was detected, thus indicating that the barrier was larger than 20−21 kcal/mol.

When subjected to reversed-phase HPLC analysis, the presence of two chromatographic peaks confirmed the existence of the *syn* and *anti* diastereoisomers, although similar retention times thwarted the physical separation. After some attempts, a cellulose-based enantioselective HPLC column (see the Experimental Section for details) was found to be effective in the resolution of the three stereoisomers (Figure 2). The red

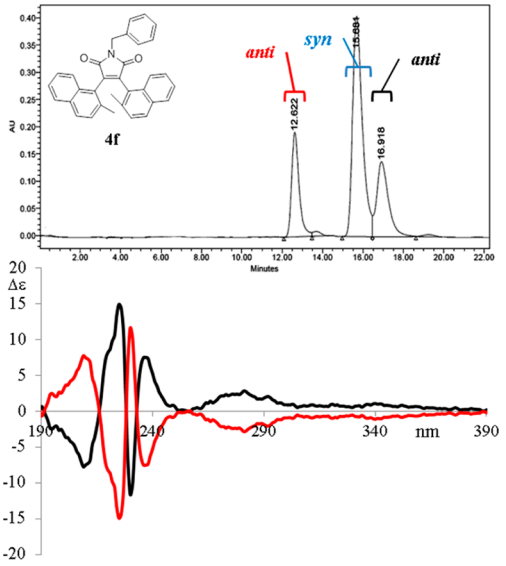

Figure 2. (Top) Chromatogram of **4f** on enantioselective HPLC column. (Bottom) Experimental ECD spectra of the first eluted stereoisomer (red trace) and of the third eluted one (black trace).

and black sections in Figure 2 (top) correspond to the two *anti* atropisomers, and the blue section identifies the *syn* (*meso*) diastereoisomer. A semipreparative HPLC approach yielded solutions that were collected and concentrated in a cold environment (−10 °C) to freeze out the *syn*/*anti* interconversion and the *anti*/*anti*′ racemization. ^{1}H NMR spectra recorded in $CDCl_3$ at −10 °C confirmed the assignment of the chromatographic peaks. As expected, the *meso* form (*syn*) showed a singlet for the benzylic CH_2 signal, while the two *anti* atropisomers were characterized by the AB system (see Figure S10 of the Supporting Information).

The kinetic portion of the interconversion process from *syn* to *anti* was performed via ^{1}H NMR. A sample of the *syn* diastereoisomer in $CDCl_3$ was kept at 46 °C, and a set of spectra were recorded at fixed intervals (180 s) until the equilibrium composition was reached. At equilibrium, a *syn*/*anti* ratio of 51/49 was observed. This ratio was confirmed by a second ^{1}H NMR spectrum of a solution of the *syn* conformer that was kept at 75 °C for 72 h. The kinetic process was analyzed at three different temperatures (46, 51, and 61 °C) (Figure S11 of the Supporting Information). From the equilibrium ratio and the slope of the regression lines, a $\Delta G^{\ddagger}$ = 24.5 kcal/mol was derived.[26] The B3LYP-computed barrier is again very close to the experimental value, the difference being less than 1.0 kcal/mol. This energy barrier corresponds to a half-life time of about 128 h at 25 °C.

3-Bromo-4-arylmaleimides. 3-Bromo-4-aryl-substituted compounds **3a−f** have been also analyzed. In these cases, only enantiomeric conformations can be generated by the single stereogenic axis due to the skewed disposition of the aryl ring. For, the benzylic group is required to detect the enantiomerization process by NMR. As in the case of compounds **4**, two transition states are available (Figure S12 of the Supporting Information). They correspond to the crossing of the *ortho*-substituent on the carbonyl group or onto the bromine (TS1 and TS2 in Table 2, respectively). DFT

Table 2. DFT-Computed Energy Barriers of 3-Aryl-4-bromo-*N*-benzylmaleimides 3a−f[a]

entry	TS1 (*ext*)	TS2 (*int*)	$\Delta G^{\ddagger}$	$\Delta\Delta G^{\ddagger b}$
3a	11.2	12.6	14.3	1.0
3b	13.6	14.6	15.3	1.1
3c	14.2	15.2	16.6	1.3
3d	15.0	15.6	17.3	1.3
3e	13.2	14.8	15.7	1.3
3f	25.8	28.2	28.6[c]	3.6

[a]The experimental energy barriers ($\Delta G^{\ddagger}$ in kcal/mol) and the difference with the corresponding 3,4-biaryl-*N*-benzylmaleimide energy barrier ($\Delta\Delta G^{\ddagger}$ in kcal/mol) are also reported. [b]This value was obtained by considering the racemization barrier of the corresponding compound **4** [c]Derived by HPLC analysis; see ref 28.

calculations suggested that the preferred pathway corresponds to the first hypothesis (i.e., TS1) and that the energy barriers were always higher with respect to the corresponding bis-aryl compounds **4**. The experimental energy barriers determined by dynamic NMR confirmed that all the racemization barriers of compounds **3** were systematically higher than those of compounds **4** ($\Delta\Delta G^{\ddagger}$ in Table 2).

These differences can be related to the steric hindrance caused by the spherical bromine in the transition state, while this effect is negligible in the ground state.[27] It is worth noting that the difference in the experimental free energies of activation ($\Delta\Delta G^{\ddagger}$ in Table 2) between mono- and bis-substituted compounds remains similar for each entry, except for compound **3f**, where it is 3.6 kcal/mol. This trend confirms that the transition state for enantiomerization does correspond to TS1, where the different steric hindrance exerted by the bromine is constant on changing the *ortho*-substituent group. Only in the case of **3f**, where both sides of the rotating aryl ring are hindered, is the $\Delta\Delta G^{\ddagger}$ much higher. In the latter case, the racemization barrier increased to 28.6 kcal/mol,[28] and the two atropisomers were fully stable at room temperature. This value is sufficiently high to allow the use of this compound in asymmetric synthesis or in the design of atropisomeric catalysts. The separation of the atropisomers was obtained by means of an amylose-enantioselective HPLC column (see the Experimental Section and Figure S13 of the Supporting Information).

■ ABSOLUTE CONFIGURATION

Having in hand the two separated atropisomers of *anti*-**4f** and **3f**, we pursued the determination of their absolute configuration. The reference method to assign the absolute configuration (AC) relies on the X-ray anomalous scattering (the "Bijovet method").[29] This approach requires the preparation of enantiopure single crystals and the presence of

dx.doi.org/10.1021/jo400200v | J. Org. Chem. 2013, 78, 3709−3719

a suitable heavy atom in the molecule (Z > Si when using Mo-Kα radiation[30]). In the present case, these requirements are not fulfilled, and the assignment by X-ray crystallography is therefore unfeasible. Moreover, during the long-lasting crystallization process, a partial isomerization of *anti*-**4f** and racemization of **3f** could take place; thus, the preparation of enantiopure crystals would not be guaranteed. Nevertheless, the determination of the AC of chiral molecules by chiro-optical techniques like optical rotation (OR), electronic circular dichroism (ECD), and vibrational circular dichroism (VCD) has recently gained feasibility and reliability thanks to the development of the time-dependent density functional theory approach (TD-DFT).[31] In the present case, the theoretical calculation of ECD spectra was selected for the absolute configuration assignment of *anti*-**4f**. In order to correctly simulate the experimental spectrum, all the available conformations should be considered, the experimental spectrum being the weighted sum of the populated conformations.[31c] The conformational search by MM methods[32] suggested that two conformations were available for the two naphthyl rings (see Figure 3).

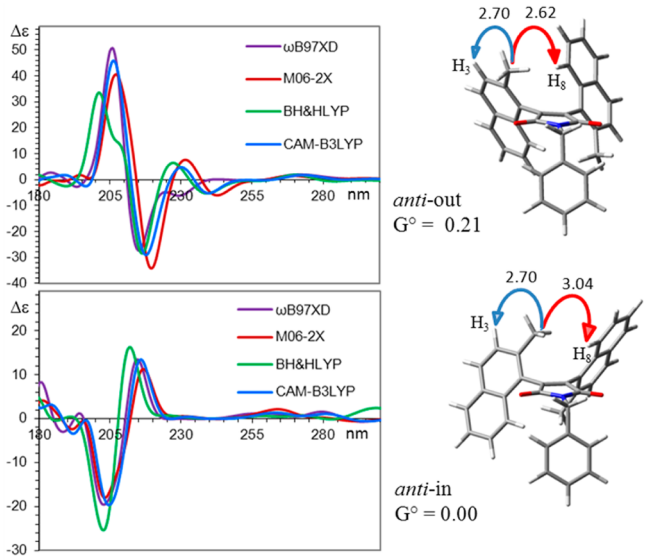

Figure 3. Theoretical ECD spectra of the two conformations of *M,M*-**4f** obtained with the TD-DFT method with four different theoretical methods and the 6-311+G(d,p) basis set. All the spectra were obtained by applying Gaussian shapes (line width =0.25 eV) to the discrete transitions. The vertical scale has been reduced by a factor of 20 with respect to the calculated value. On the right are reported the two optimized structures (relative ZPE-corrected free energies in kcal/mol, distances in Å).

In one of these, the methyl groups point toward the second ring (*anti*-in, as from Scheme 3) and in the other one they are directed toward the two carbonyl oxygens (*anti*-out in Scheme 3). In addition, two different dispositions of the benzyl group had to be considered (i.e., that where the phenyl was perpendicular to the maleimide ring and a second where the phenyl ring had a dihedral of 30° with the plane of maleimide). After minimization by DFT at the B3LYP/6-31G(d) level, the *anti*-in and *anti*-out conformations were found to have very similar energy and only the perpendicular conformation of the benzyl group was found to be essentially populated (see Figure 3). The electronic excitation energies and rotational strengths were calculated in the gas phase using TD-DFT with four different functionals to explore whether different types of calculations provide different shapes of the simulated spectra. Simulations were performed on the previously optimized geometries using the hybrid functionals BH&HLYP[33] and M06-2X,[34] the long-range correlated ωB97XD that includes empirical dispersion,[35,36] and CAM-B3LYP that includes long-range correction using the coulomb attenuating method.[37] Three explorative tests were performed using different basis sets that proved to be accurate for these calculations such as the 6-311++G(2d,p),[38] def2-TZVPP,[39] and 6-311+G(d,p)[38] basis sets with the CAM-B3LYP functional, without appreciable differences (see Figure S14 of the Supporting Information). For this reason, all of the calculations employed the computationally cheaper 6-311+G(d,p) basis set. Rotational strengths were calculated in both length and velocity representation, the resulting values being very similar (RMS differences <5%). For this reason, the errors due to basis set incompleteness should be very small or negligible.[40]

As shown in Figure 3, the simulated ECD spectra for the two conformations of the *M,M* atropisomer are very similar within the same conformation, but the two conformations exhibit nearly opposite spectra. For this reason, the conformationally averaged ECD spectrum will be extremely sensitive to the population ratio, and a knowledge of the experimental ratio of the two conformers is necessary to obtain a correct simulation.[41] A direct detection of the experimental ratio of the two conformations was impossible, being the π-barrier inaccessible to the dynamic-NMR technique. Thus, NOE spectra were used to experimentally evaluate this ratio (see Figure 4).[42] In both the *anti*-in and *anti*-out conformers, the 2-

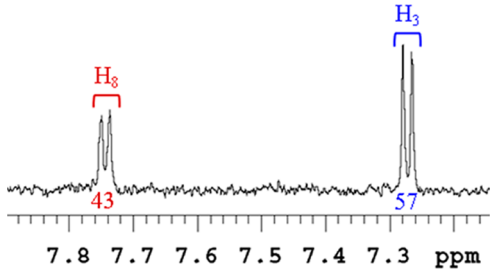

Figure 4. DPFGSE-NOE spectra of **4f** obtained by saturation of the 2-methyl groups (600 MHz in CD_3CN, mixing time =1.5 s). The numbers over the scale represent the normalized integration of the two NOE peaks. Spectra obtained with different mixing times are reported in the Supporting Information.

methyl group of each naphthyl ring is spatially close to the hydrogen in position 3 of the same ring (blue arrows in Figure 3, right) and to the H_8 of the second naphthyl ring (red arrows in Figure 3, right).

Depending on the conformation considered,[43] the distances from the 2-methyl to H_8 are different, while the Me−H_3 distance is the same (2.70 Å). The NOE effect on H_3 can thus act as an internal "control" distance. In the *anti*-in conformation the Me−H_3/Me−H_8 distance ratio was calculated as 0.89, whereas in the *anti*-out conformation the same ratio was 1.03 (Figure 3). The experimental NOE ratio observed by saturating the 2-methyl signal (Figure 4) is in between the two limiting values (0.93_5); thus, both conformations must be appreciably populated. If the calculated distances are taken into account, the observed NOE

dx.doi.org/10.1021/jo400200v | J. Org. Chem. 2013, 78, 3709−3719

corresponds to a 60:40 (±15%) ratio of the two conformations (*anti*-in:*anti*-out). This result is in agreement with the 59:41 ratio based on the computed free energies of the two conformations (0.00 and 0.21 kcal/mol for the *anti*-in and *anti*-out, respectively).

The experimental ECD spectra of **4f** (Figure 2, bottom) show the characteristic features of the 1-naphthyl chromophore in that a weak structured band at 285 nm and intense bands at about 225 nm are observed.[44] These Cotton effects are certainly due to the ^1L_a and ^1B transitions,[45] polarized along the short and long axis of the naphthalene chromophore, respectively. Below 220 nm the absorption due to the ^1B transition of the benzyl moiety can also be observed. The structured region between 240 and 210 nm and in particular the narrow negative band at 231 nm could be the result of two opposite exciton couplings involving the ^1B transition of the two naphthalene rings.[46]

In the *anti*-in conformation, the two dipoles of the naphthalene rings form a positive dihedral angle while in the *anti*-out they form a negative angle (see Figure 5). To confirm

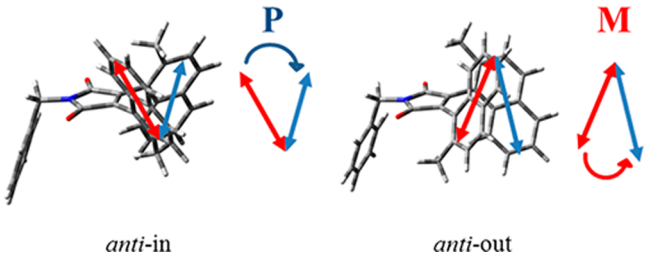

Figure 5. Orientations of the ^1B transitions of the two naphthyl rings of **4f** for the *anti*-in and *anti*-out conformations.

this hypothesis and to exclude any contribution of the benzyl group, we simulated the ECD spectrum of the 3,4-bis-(2-methylnaphthyl) maleimide. The simulated spectra are identical to that previously obtained for **4f**. In addition, the analysis of the molecular orbitals involved in the electronic transitions between 230 and 200 nm showed that they are localized mostly on the naphthyl rings (Figures S16 and S17 of the Supporting Information). When the simulated ECD spectrum of the *M,M* atropisomer was generated taking into account the ratio suggested by calculations (blue, green, red, and purple lines in Figure 6), the matching with the experimental ECD spectrum of the second eluted atropisomer of **4f** is quite good, the best simulation being obtained with the ωB97XD functional.[47] To further confirm the reliability of the assignment, the population ratio of the two conformations was changed by ±20% without appreciable worsening of the simulation (see Figure S18 of the Supporting Information). It is therefore concluded that the first eluted enantiomer of **4f** corresponds to the *P,P* atropisomer and the second eluted to the *M,M* atropisomer.[48]

Using the same approach applied to compound **4f**, the absolute configuration of **3f** was determined by the simulation of the ECD spectra. Four different conformations were found to be populated by MM conformational search. Because of the presence of a single naphthyl ring, they correspond to the two dispositions of the naphthyl ring already discussed before, combined with the two available dispositions of the benzyl ring (Figure S20 of the Supporting Information). The experimental ECD spectrum shows two opposite Cotton effects that are probably coupled together. At variance with compound **4f**, this

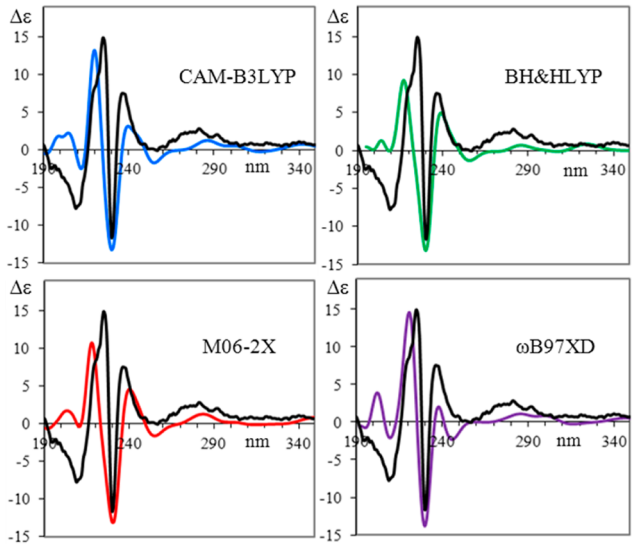

Figure 6. Computed ECD spectra of **4f** considering a ratio of 59:41 of the two conformations, and using different functionals. All the calculations employed the 6-311+G(d,p) basis set. Black line: experimental ECD spectrum of the second eluted atropisomer of **4f**.

single exciton coupling could be due to the stereogenic axis generated by the naphthyl ring and the maleimide chromophore or by the naphthyl ring with the benzyl group. The ECD spectra simulated for the four conformations assuming the *M* absolute configuration exhibit different shapes, in particular in the 230 nm region. To understand whether the 230 nm region of the spectrum was due to the transitions related to maleimide, the MO components of the most intense UV transition calculated in that region (231 nm) were generated and visualized for the four conformations (Figures S21−S24 of the Supporting Information). The occupied MO involved were localized mainly on the maleimide ring, whereas the unoccupied orbital corresponded to the LUMO orbital, again localized exclusively on maleimide. Regarding the second transition calculated at 211 nm, MO analysis confirmed that it was due to the ^1B transition of the naphthalene ring. No significant contribution due to the benzyl ring was observed for both transitions. For this reason, the observed ECD spectrum can be discussed in terms of two chromophores disposed in a well-defined arrangement.

Thus, the spectrum shown in Figure 7, showing a negative exciton coupling, can be related to the *M* atropisomer of **3f**.[49] This assignment is further supported by the simulation obtained assuming Boltzmann statistics on the spectra simulated for the four conformation (30:26:24:21 ratio, as from Boltzmann statistics using ZPE corrected free energies). The experimental ECD spectrum showed that the intensity ratio between the weak band at 285 nm and the strong band of naphthalene at 221 nm is very small (as usually happens), whereas the same ratio was much larger in the case of the ECD spectrum of **4f** (see Figure 2). This feature further confirms that the spectrum of **4f** was dominated by the two opposite exciton couplings due to the *anti*-in and *anti*-out conformations, that reduced the intensity of the CD spectrum of the naphthalene transitions in the 225 nm region.

CONCLUSIONS

The planar scaffold of maleimide provides separable atropoisomers when hindered aryl rings occupy to the 3,4 positions,

dx.doi.org/10.1021/jo400200v | J. Org. Chem. 2013, 78, 3709−3719

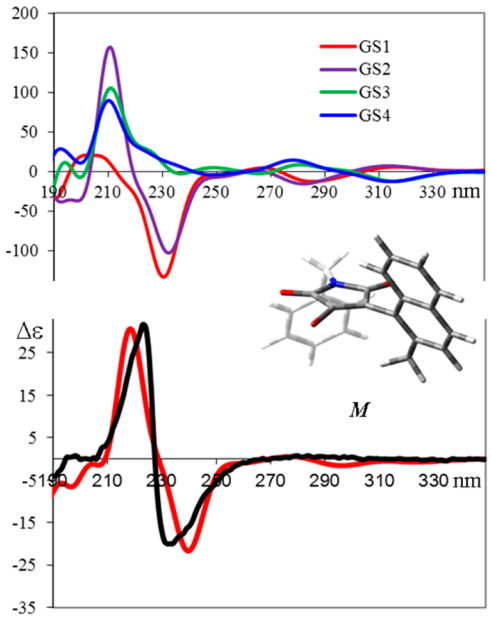

Figure 7. (Top) Calculated ECD spectra for the four possible conformations of **3f**. Calculations at the CAM-B3LYP/6-311+G(d,p) level. (Bottom) Simulated (red trace) and experimental spectrum (black trace) of the first eluted atropisomer of **3f**.

and 3-bromo-4-arylmaleimides generate atropisomers as well. The latter can be further functionalized and take advantage of the larger racemization barrier. DFT calculations at the B3LYP/6-31G(d) level were able to predict the energy barriers for racemization with good accuracy, and can help in the design of new atropisomeric compounds to be used in asymmetric synthesis. The absolute configuration of the most hindered compounds was determined by theorethical simulation of the ECD spectrum by means of TD-DFT calculations supported by NMR conformational analysis.

EXPERIMENTAL SECTION

Materials. 3,4-Dibromo-1*H*-pyrrole-2,5-dione, benzyl bromide, 1-bromo-2-methylnaphthalene, *n*-butyllithium, and the boronic acids **2a**–**e** were commercially available. 2-Methylnaphthylboronic acid[50] and 3,4-dibromo-1-benzylpyrrole-2,5-dione[51] were prepared according to known procedures. Diethyl ether and THF have been dried before use by distillation on Na/benzophenone. Chromatography employed the following stationary phases: silica gel 60 F254 for the TLC and silica gel 60 Å (230–400 mesh) for prepurification. All reactions were performed in dried glassware and under dry nitrogen atmosphere. Glassware was dried at 70 °C for at least 3 h immediately before use. A Phenomenex Luna C18 (10 μm, 100 Å, 250 × 21.2 mm) semipreparative column was used to purify the compounds using mixtures of CH_3CN and H_2O as eluent. Enantioselective HPLC columns were used to separate the stable atropisomers of **4f** and **3f** (Phenomenex LUX-cellulose-2 250 × 10 mm and Daicel Chiralpak AD-H 250 × 21.2 mm, respectively). Detection wavelength was 254 nm.

NMR spectra were recorded using a spectrometer operating at a field of 14.4 T (600 MHz for ^{1}H, 150.8 for ^{13}C). Chemical shifts are given in ppm relative to the internal standards tetramethylsilane (^{1}H and ^{13}C) or relative to the residual peak of the solvents. The 600 MHz ^{1}H spectra were acquired using a 5 mm dual direct probe with a 9000 Hz spectral width, 2.0 μs (20° tip angle) pulse width, 3 s acquisition time, and 1 s delay time. A shifted sine bell weighting function equal to the acquisition time (i.e., 3 s) was applied before the Fourier transformation. The 150.8 MHz ^{13}C spectra were acquired under proton decoupling conditions with a 38000 Hz spectral width, 4.2 μs (60° tip angle) pulse width, 1 s acquisition time and 1 s delay time. A line broadening function of 1–2 Hz was applied before the Fourier transformation. Assignment of the carbons multiplicity were obtained by means of the DEPT sequences.

General Synthetic Procedure. 1-Benzyl-3,4-dibromo-1*H*-pyrrole-2,5-dione (**1**) (1 mmol) was dissolved in dry THF (5 mL), and then the appropriate boronic acid (2 mmol), cesium carbonate (2.5 mmol), and the palladium catalyst $Pd(PPh_3)_4$ or $Pd(OAc)_2$ were added. The stirred solution was kept at reflux for 2 h or at 40 °C overnight (Table 3 summarizes the experimental conditions). Et_2O and H_2O were then added, and the extracted organic layer was dried (Na_2SO_4), filtered on silica gel, and concentrated at reduced pressure. The crude products were purified by semipreparative HPLC on C18 column to obtain analytically pure samples of **3a**–**f** and **4a**–**f**.

Table 3. Summary of the Synthetic Details

entry (yield, %)	entry (yield, %)	catalyst	temp (°C)	time (h)
3a (30)	**4a** (32)	$Pd(PPh_3)_4$	reflux	2
3b (37)	**4b** (18)	$Pd(OAc)_2$	40	overnight
3c (35)	**4c** (30)	$Pd(OAc)_2$	reflux	2
3d (27)	**4d** (10)	$Pd(PPh_3)_4$	40	overnight
3e (28)	**4e** (20)	$Pd(OAc)_2$	reflux	2
3f (13)	**4f** (6)	$Pd(OAc)_2$	reflux	2

*1-Benzyl-3-bromo-4-(o-tolyl)-1H-pyrrole-2,5-dione (**3a**).* Yield: 0.104 g (30%) as a white waxy solid. ^{1}H NMR (600 MHz, CD_2Cl_2, 5.33 ppm, 25 °C): δ 2.27 (s, 3H), 4.79 (s, 2H), 7.22 (d, *J* = 7.7 Hz, 1H), 7.28–7.44 (m, 8H). ^{13}C NMR (150.8 MHz, CD_2Cl_2, 54.0 ppm, 25 °C): δ 20.6 (CH_3), 43.1 (CH_2),12.3 (CH), 127.1 (Cq), 128.0 (Cq), 128.5 (CH), 128.9 (2CH), 129.3 (2CH), 129.8 (CH), 130.8 (CH), 131.3 (CH), 136.6 (Cq), 137.7 (Cq), 144.3 (Cq), 165.7 (Cq), 168.6 (Cq). HPLC: CH_3CN/H_2O 82:18 v/v, t_R = 7.78 min. HRMS (EI): *m*/*z* calcd for $C_{18}H_{14}BrNO_2$ [$M^{\bullet+}$] 355.02079, found 355.0210.

*1-Benzyl-3,4-di-o-tolyl-1H-pyrrole-2,5-dione (**4a**).* Yield: 0.118 g (32%) as a white amorphous solid. ^{1}H NMR (600 MHz, CD_2Cl_2, 5.33 ppm, 25 °C): δ 2.06 (s, 6H), 4.84 (s, 2H), 7.09 (d, *J* = 7.6 Hz, 2H), 7.17 (t, *J* = 7.6 Hz, 2H), 7.21 (d, *J* = 7.6 Hz, 2H), 7.29 (td, *J* = 7.6, 1.1 Hz, 2H), 7.31- 7.35 (m, 1H), 7.38 (t, *J* = 7.43 Hz, 2H), 7.44 (d, *J* = 7.1 Hz, 2H). ^{13}C NMR (150.8 MHz, CD_2Cl_2, 54.0 ppm, 25 °C): δ 20.6 (2 CH_3), 42.6 (CH_2), 126.2 (2 CH), 128.3 (CH), 128.7 (2 CH), 129.2 (2 CH), 129.4 (2 Cq), 130.1 (2 CH), 130.6 (bs, 2 CH), 131.2 (2 CH), 137.3 (2 Cq), 137.7 (Cq), 141.1 (2 Cq), 170.8 (2 Cq). HPLC: CH_3CN/H_2O 82:18 v/v, t_R = 10.58 min. HRMS (EI): *m*/*z* calcd for $C_{25}H_{21}NO_2$ [$M^{\bullet+}$] 367.15723, found 367.1572.

*1-Benzyl-3-bromo-4-(2-ethylphenyl)-1H-pyrrole-2,5-dione (**3b**).* Yield: 0.135 g (37%) as a white waxy solid. ^{1}H NMR (600 MHz, $C_2D_2Cl_4$, 6.00 ppm, 25 °C): δ 1.17 (t, *J* = 7.5 Hz, 3H), 2.55 (q, *J* = 7.5 Hz, 2H), 4.80 (bs, benzylic CH_2), 7.18 (d, *J* = 7.6 Hz, 1H), 7.30- 7.42 (m, 7H), 7.48 (t, *J* = 7.6, 1H). ^{13}C NMR (150.8 MHz, $C_2D_2Cl_2$, 74.0 ppm, 25 °C): δ 15.25 (CH_3), 26.9 (CH_2), 42.8 (CH_2), 126.1 (CH), 126.6 (Cq), 126.9 (CH), 128.3 (CH), 128.6 (CH), 129.0 (2 CH),129.4 (CH), 130.7 (Cq), 135.8 (Cq), 143.1 (Cq), 144.2 (Cq), 165.2 (Cq), 168.4 (Cq). HPLC: CH_3CN/H_2O 82:18 v/v, t_R = 9.25 min. HRMS (EI): calcd for $C_{19}H_{16}BrNO_2$ [$M^{\bullet+}$] 369.03644, found 369.0360.

*1-Benzyl-3,4-bis(2-ethylphenyl)-1H-pyrrole-2,5-dione (**4b**).* Yield: 0.070 g (18%) as a white amorphous solid.^{1}H NMR (600 MHz, CD_3CN, 1.96 ppm, 60 °C): δ 1.07 (t, *J* = 7.6 Hz, 6H), 2.49 (q, *J* = 7.6 Hz, 4H), 4.82 (s, 2H), 7.11 (d, *J* = 7.7 Hz, 2H), 7.17 (t, *J* = 7.6 Hz, 2H), 7.30–7.37 (m, 5H), 7.40 (bd, 4H). ^{13}C NMR (150.8 MHz, CD_3CN, 118.3 ppm, 60 °C): δ 15.2 ($2CH_3$), 27.3 ($2CH_2$), 43.1 (CH_2), 126.8 (2CH), 128.8 (2CH),128. Eight (CH), 129.6 (2Cq), 129.7 (2CH), 129.9 (2CH), 130.9 (2CH), 131.3 (2CH), 138.4 (Cq), 142.6 (2Cq), 144.5 (2Cq), 171.9 (2Cq). HPLC: CH_3CN/H_2O 82:18 v/v, t_R = 15.10 min. HRMS (EI): *m*/*z* calcd for $C_{27}H_{25}NO_2$ [$M^{\bullet+}$] 395.18853, found 395.1881.

dx.doi.org/10.1021/jo400200v | J. Org. Chem. 2013, 78, 3709–3719

*1-Benzyl-3-bromo-4-(2,3-dimethylphenyl)-1H-pyrrole-2,5-dione (**3c**).* Yield: 0.130 g (35%) as a white waxy solid. ^{1}H NMR (600 MHz, $C_2D_2Cl_4$, 6.00 ppm, 25 °C): δ 2.16 (s, 3H), 2.35 (S, 3H), 4.78 (d, J = 14.59 Hz, 1H), 4.82 (d, J = 14.59 Hz, 1H), 7.09 (d, J = 7.6 Hz, 1H), 7.23$_5$ (t, J = 7.6 Hz, 1H), 7.28−7.44 (m, 6H). ^{13}C NMR (150.8 MHz, $C_2D_2Cl_4$, 74.0 ppm, 25 °C): δ 18.0 (CH_3), 20.5 (CH_3), 42.7 (CH_2), 125.8 (CH), 126.3 (Cq), 127.1 (CH), 128.3 (2 CH), 129.0 (2 CH), 132.0 (Cq), 135.6 (Cq), 135.8 (Cq), 138.2 (Cq), 144.2 (Cq), 165.3 (Cq), 168.5 (Cq). HPLC: CH_3CN/H_2O 82:18 v/v, t_R = 9.20 min. HRMS (EI): m/z calcd for $C_{19}H_{16}BrNO_2$ [$M^{\bullet+}$] 369.03644, found 369.0358.

*1-Benzyl-3,4-bis(2,3-dimethylphenyl)-1H-pyrrole-2,5-dione (**4c**).* Yield: 0.118 g (30%) as a white amorphous solid. ^{1}H NMR (600 MHz, $CDCl_3$, 50 °C): δ 1.96 (s, 6H), 2.22 (s, 6H), 4.83 (s, 2H), 6.88 (bd, 2H), 7.02 (bt, 2H), 7.12 (bd, 2H), 7.21−7.40 (m, 3H), 7.45 (bd, 2H). ^{13}C NMR (150.8 MHz, $CDCl_3$, 77.0 ppm, 50 °C): δ 17.4 (2 CH_3), 20.2 (2 CH_3), 42.2 (CH_2), 125.5 (2 CH), 127.8 (3 CH), 128.6 (2 CH), 128.7 (2 CH), 128.9 (2 Cq), 131.0 (2 CH), 135.4 (2 Cq), 136.7 (Cq),137.4 (2 Cq), 141.2 (2 Cq), 170.4 (2 Cq). HPLC: CH_3CN:H_2O 82:18 v/v, t_R = 14.51 min. HRMS (EI): m/z calcd for $C_{27}H_{25}NO_2$ [$M^{\bullet+}$] 395.18853, found 395.1880.

*1-Benzyl-3-bromo-4-(2-isopropylphenyl)-1H-pyrrole-2,5-dione (**3d**).* Yield: 0.104 g (27%) as a white waxy solid. ^{1}H NMR (600 MHz, $C_2D_2Cl_4$, 6.00 ppm, 25 °C): δ 1.18 (d, J = 6.7 Hz, 3H), 1.24 (d, J = 6.7 Hz, 3H), 2.69 (sett, J = 6.7 Hz, 1H), 4.77 (d, J = 14.6 Hz, 1H), 4.81 (d, J = 14.6 Hz, 1H), 7.13 (d, J = 7.7 Hz, 1H), 7.30 (t, J = 7.5 Hz, 1H), 7.32−7.42 (m, 5H), 7.43−7.52 (m, 2H). ^{13}C NMR (150.8 MHz, $C_2D_2Cl_4$, 74.0 ppm, 25 °C): δ 23. Nine (CH_3), 24.5 (CH_3), 31.9 (CH), 42.8 (CH_2), 126.0 (Cq), 126.1 (CH), 126.2 (CH), 127.1 (Cq), 128.3 (CH), 128.6 (2CH), 129.0 (2CH), 129.2 (CH), 130.8 (CH), 135.8 (Cq), 144.6 (Cq), 148.0 (Cq), 165.2 (Cq), 168.5 (Cq). HPLC: CH_3CN/H_2O 82:18 v/v, t_R = 12.15 min. HRMS (EI): m/z calcd for $C_{20}H_{18}BrNO_2$ [$M^{\bullet+}$] 383.05209, found 383.0525.

*1-Benzyl-3,4-bis(2-isopropylphenyl)-1H-pyrrole-2,5-dione (**4d**).* Yield: 0.042 g (10%) as a white amorphous solid. NMR spectra showed the presence of the two conformations *syn* (49%) and *anti* (51%). ^{1}H NMR (600 MHz, $CDCl_3$, 0 °C): δ 0.72 (d, 6H *anti*, J = 6.4 Hz), 0.81 (d, 6 H *syn*, J = 6.4 Hz), 1.14$_5$ (d, 6 H *anti*, J = 6.4 Hz), 1.22 (d, 6 H *syn*, J = 6.4 Hz), 2.65 (quint, 2H *anti*, J = 6.4 Hz), 2.70 (quint, 2 H *syn*, J = 6.8 Hz), 4.79 (d, 1H *anti*, J = 14.5 Hz), 4.83$_5$ (s, 2 H *syn*), 4.88 (d, 1 H *anti*, J = 14.5 Hz), 6.99 (bt, 4 H), 7.08−7.16 (m, 4 H), 7.24−7.40 (m, 14 H), 7.49 (bt, 4 H). ^{13}C NMR (150.8 MHz, $CDCl_3$, 77.0 ppm, 0 °C): δ 23.0 (2 CH_3), 23.2 (2 CH_3), 24.7 (2 CH_3), 25.1 (2 CH_3), 31.1 (4 CH), 42.1$_5$ (CH_2), 42.2 (CH_2), 125.6 (2CH), 125.7 (2CH), 126.1 (2CH), 126.4 (2CH), 126.6 (2 Cq), 126.7 (2Cq), 127.8 (2 CH), 128.7 (4 CH), 128.8 (2 CH), 128.9 (2CH), 129.8 (2CH), 129.9 (2CH), 129.9 (2CH), 130.4 (2CH), 136.4 (2 Cq), 136.5 (2 Cq), 140.3 (2 Cq), 140.6 (2 Cq), 147.7 (2 Cq), 148.0 (2 Cq), 170.6 (4 Cq). HPLC: CH_3CN/H_2O 82:18 v/v, t_R = 21.34 min. HRMS (EI): m/z calcd for $C_{29}H_{29}NO_2$ [$M^{\bullet+}$] 423.21983, found 423.2192

*1-Benzyl-3-bromo-4-(naphthalen-1-yl)-1H-pyrrole-2,5-dione (**3e**).* Yield: 0.110 (28%) g as a white amorphous solid. ^{1}H NMR (600 MHz, $CDCl_3$, 25 °C): δ 4.85 (s, 2H), 7.29−7.4 (m, 3H), 7.46 (d, J = 7.2 Hz, 2H), 7.48−7.63 (m, 5H), 7.92 (d, J = 8.3 Hz, 1H), 7.99$_5$ (d, J = 8.3 Hz, 1H). ^{13}C NMR (150.8 MHz, $CDCl_3$, 77.0 ppm, 25 °C): δ 42.8 (CH_2), 124.9 (CH), 125.0 (Cq), 125.5 (CH), 126.5 (CH),126.8 (CH), 127.1 (Cq), 128.2 (CH), 128.5 (CH), 128.8$_1$ (CH), 128.8$_3$ (2CH), 128.9 (2CH), 129.9 (Cq), 131.1 (CH), 133.6 (Cq), 135.8 (Cq), 142.4 (Cq), 165.1 (Cq), 168.4 (Cq). HPLC: CH_3CN/H_2O 90:10 v/v, t_R = 5.94 min. HRMS (ESI-Orbitrap): m/z calcd for $C_{21}H_{15}BrNO_2^+$ [M + H^+] 392.02807, found 392.02914.

*1-Benzyl-3,4-di(naphthalen-1-yl)-1H-pyrrole-2,5-dione (**4e**).* Yield: 0.088 g (20%) as a white amorphous solid. ^{1}H NMR (600 MHz, $C_2D_2Cl_4$, 6.00 ppm, 60 °C): δ 4.92 (s, 2H), 7.24 (t, J = 7.6 Hz, 2H), 7.32−7.38 (m, 7H), 7.40 (t, J = 7.6 Hz, 2H), 7.50 (d, J = 7.6 Hz, 2H), 7.59 (bd, 2H), 7.74 (d, J = 8.1 Hz, 2H), 7.78 (d, J = 7.6 Hz, 2H). ^{13}C NMR (150.8 MHz, $C_2D_2Cl_4$, 74.0 ppm, 60 °C): δ 42.5 (CH_2), 125.1 (2 CH), 125.2 (2 CH), 126.1 (2 CH), 126.4 (2 CH), 126.6 (2 Cq), 127.9 (CH), 128.4 (2 CH), 128.5 (2 CH), 128.7 (2 CH), 128.8 (2 CH), 130.3 (2 CH), 130.7 (2 Cq), 133.4 (2 Cq), 136.5 (Cq), 140.4 (2 Cq), 170.4 (2 Cq). HPLC: CH_3CN:H_2O 90:10 v/v, t_R = 7.23 min. HRMS (ESI-Orbitrap): m/z calcd for $C_{31}H_{22}NO_2^+$ [M + H^+] 440.16451, found 440.16529.

*1-Benzyl-3-bromo-4-(2-methylnaphthalen-1-yl)-1H-pyrrole-2,5-dione (**3f**).* Yield: 0.053 g (13%) as white amorphous solid. ^{1}H NMR (600 MHz, $CDCl_3$, 25 °C): δ 2.37 (s, 3H), 4.87 (s, 2H), 7.30−7.36 (m, 1H), 7.37−7.40 (m, 2H), 7.41−7.49 (m, 6H), 7.86−7.90 (m, 2H). ^{13}C NMR (150.8 MHz, $CDCl_3$, 77.0 ppm, 25 °C): δ 20.6 (CH_3), 42.8 (CH_2), 123.2 (Cq), 124.3 (CH), 125.6 (CH),127.0 (CH), 128.1 (CH), 128.4 (CH), 128.5 (3CH), 128.8 (2CH), 129.2 (Cq), 130.2 (CH), 130.6 (Cq), 131.8 (Cq), 135.2 (Cq), 135.8 (Cq), 143.6 (Cq), 164.9 (Cq), 168.0 (Cq). ChiralPak AD-H (5 μm, 250 × 20 mm, 20 mL/min, 254 nm, 25 °C) semipreparative HPLC column has been used for the separation of the atropisomers and for the kinetic study; hexane/2-propanol 90:10 v/v, t_R 6.89 and 9.55 min. HRMS (ESI-Orbitrap): m/z calcd for $C_{22}H_{17}BrNO_2^+$ [M + H^+] 406.04372, found 406.04453.

*1-Benzyl-3,4-bis(2-methylnaphthalen-1-yl)-1H-pyrrole-2,5-dione (**4f**).* Total yield (as *syn anti*): 0.028 g (6%) as slightly yellow waxy solid. *Syn.* ^{1}H NMR (600 MHz, $CDCl_3$, −10 °C): δ 2.24 (s, 6H), 4.95 (s, 2H), 7.12 (t, J = 7.6 Hz, 2H), 7.20 (d, J = 8.3, 2H), 7.27−7.29 (m, 2H), 7.34−7.42 (m, 3H), 7.51 (d, J = 7.0 Hz, 2H), 7.60 (d, J = 8.6 Hz, 2H), 7.64−7.70 (m, 4H). ^{13}C NMR (150.8 MHz, $CDCl_3$, 77.00 ppm, −10 °C): δ 21.13 (CH_3), 42.29 (CH_2), 124.30 (2Cq), 124.80 (2CH), 125.06 (2CH), 126.11 (2CH), 127.86 (CH), 128.15 (2CH), 128.45 (2CH), 128.59 (2CH), 128.80 (2CH), 129.71 (2CH), 131.00 (2Cq), 131.58 (2Cq), 135.41 (2Cq), 136.44 (Cq), 141.92 (2Cq), 170.13 (2Cq). *Anti.* ^{1}H NMR (600 MHz, $CDCl_3$, −10 °C): δ 2.03 (s, 6H), 4.95 (AB system, J = 14.7$_5$ Hz, 2H), 7.15 (d, J = 8.44 Hz, 2H), 7.27−7.42 (m, 7H), 7.52 (d, J = 7.73 Hz, 2H), 7.56 (d, J = 7.73 Hz, 2H), 7.69 (d, J = 8.5 Hz, 2H), 7.72−7.76 (m, 2H). ^{13}C NMR (150.8 MHz, $CDCl_3$, 77.0 ppm, −10 °C): δ 21.5 (CH_3), 42.3 (CH_2), 124.1 (2Cq), 125.0 (2CH), 125.2 (2CH), 126.2 (2CH),127.9 (CH), 128.3 (2CH), 128.5 (2CH), 128.6 (2CH), 128.8 (2CH), 129.7 (2CH), 131.0 (2Cq), 131.7 (2Cq), 136.0 (2Cq), 136.4 (Cq), 142.2 (2Cq), 170.3 (2Cq). Lux Cellulose-2 HPLC column was used to separate the three stereoisomers. (5 μm, 100 Å, 250 × 10.00 mm, hexane/2-propanol 90:10 v/v, 5 mL/min, detection at 254 nm, 25 °C); t_R *syn* = 15.88 min, t_R *anti:* 12.62 and 16.92 min. HRMS (ESI-Orbitrap): m/z calcd for $C_{33}H_{26}NO_2^+$ [M + H^+] 468.19581, found 468.19726.

Variable-Temperature NMR Spectra. The low-temperature spectra were obtained by using a flow of dry nitrogen which entered into an inox steel heat-exchanger immersed in liquid nitrogen and connected to the NMR probe head by a vacuum-insulated transfer line. Temperature calibrations were performed before the experiments using a digital thermometer and a Cu/Ni thermocouple placed in an NMR tube filled with isopentane. The conditions were kept as equal as possible with all subsequent work. The uncertainty in the temperature measurements can be estimated from the calibration curve as ±1 °C. The spectra above ambient temperature were calibrated by the same thermocouple placed in a NMR sample filled with tetrachloroethane. The uncertainty in the high-temperature range can be estimated from the calibration curve as ±1 °C. Line-shape simulations were performed using a PC version of the QCPE DNMR6 program.[52] Electronic superimposition of the original and the simulated spectra enabled the determination of the most reliable rate constants at a few different temperatures. These constants provided the free energies of activation ($\Delta G^{\ddagger}$) by means of the Eyring equation.[53] Within the experimental uncertainty, the latter values were found essentially invariant in the examined temperature range, thus implying an almost negligible activation entropy $\Delta S^{\ddagger}$, as observed in the majority of conformational processes investigated by dynamic NMR.[7] The NOE experiments on *anti*-**4f** were performed in CD_3CN at 10 °C by means of the DPFGSE-NOE sequence.[54] To selectively irradiate the methyl signal, a 50 Hz wide shaped pulse was calculated with a refocusing-SNOB shape and a pulse width of 37 ms. Six spectra using different mixing times (0.25, 0.5, 0.75, 1.0, 1.25, and 1.5 s) were acquired to provide the growing curve of the NOEs. In the observed range the grow was linear, and the average NOE ratio between the two aromatic peaks shown in Figure 4 was 57:43.

ECD Spectra. ECD spectra were recorded at 25 °C in acetonitrile solutions. The concentrations of the samples were tuned to obtain a maximum absorbance of about 0.8 in the UV spectrum using a 0.2 cm path length. Final concentrations were 2×10^{-5} M and 5×10^{-5} M for **4f** and **3f**, respectively. Spectra were recorded in the 190−400 nm interval, and four scans were summed. Reported $\Delta\varepsilon$ values are expressed as L $mol^{-1}cm^{-1}$.

Calculations. The conformational searches were preliminarily carried out by means of the Molecular Mechanics Force Field (MMFF), using the Monte Carlo methods.[32] The most stable conformers thus identified were subsequently by DFT computations, that were performed by the Gaussian 09 rev A.02 series of programs[23] using standard optimization parameters. All of the calculations employed the B3LYP hybrid HF-DFT method[55] and the 6-31G(d) basis sets. Harmonic vibrational frequencies were calculated for all the stationary points. As revealed by the frequency analysis, imaginary frequencies were absent in all ground states whereas one imaginary frequency was associated with each transition state. Visual inspection of the corresponding normal mode[56] validated the identification of the transition states. The energy values listed in Tables 1 and 2 derive from total electronic energies. In general, these give the best fit with experimental DNMR data,[57] and for this reason the computed values have not been corrected for zero-point energy contributions or other thermodynamic parameters. This approach avoids artifacts due to the ambiguous choice of the adequate reference temperature and from the idealization of low-frequency vibrators as harmonic oscillators.[58]

ECD Simulations. The ECD spectra of *anti*-**4f** and **3f** were simulated by means of TD-DFT calculations. The electronic excitation energies and rotational strengths have been calculated in the gas phase using the geometries obtained at the B3LYP/6-31G(d) level with the CAM-B3LYP,[37] BH&HLP,[33] M06-2X,[34] and ωB97XD[35] functionals. All of the calculations employed the 6-311+G(d,p) basis set. Explorative simulations were performed also with the 6-311++G(2d,p) and def2/TZVPP basis sets. Rotational strengths were calculated in both length and velocity representation, the resulting values being very similar (differences below 5%). For this reason, BSSE errors should be very small.[40] The simulated spectra were obtained using the first 70 calculated transitions (lowest wavelength about 150 nm) and applying a 0.25 eV line width. The simulated spectra resulting from the Boltzmann-averaged sum of the conformations were red-shifted by 10−15 nm to get the best simulations with the experimental spectra.

■ ASSOCIATED CONTENT

Supporting Information

VT spectra of **3a−e** and **4a−c,e**; NMR spectra of the two diastereoisomers of **4f**; kinetic data for the *syn*/*anti* interconversion of **4f**; stereodynamic pathways of compounds **3**; enantioselective HPLC of compound **3f**; simulated ECD spectra of the two conformations of **4f**; molecular orbitals of the *anti*-in and *anti*-out conformation of **4f** involved in the three strongest CD transitions; simulations of the experimental ECD spectrum of the second eluted enantiomer of **4f** using different ratios of the two conformations; NOE spectra of *anti*-**4f** with different mixing times; simulated and experimental VCD spectrum of **4f**; 3D views of the four conformations of compound **3f**; molecular orbitals of the GS1, GS2, GS3, and GS4 conformations of **3f** involved in the CD transitions calculated at 231 and 211 nm; computational details of **3a−f** and **4a−f**; ^{1}H and ^{13}C NMR spectra of **3a−f** and **4a−f**. This material is available free of charge via the Internet at http://pubs.acs.org.

■ AUTHOR INFORMATION

Corresponding Author

*E-mail: andrea.mazzanti@unibo.it.

Notes

The authors declare no competing financial interest.

■ ACKNOWLEDGMENTS

Financial support was received from the University of Bologna (RFO funds 2010 and 2011). We thank Professor Lodovico Lunazzi for helpful discussions and proofreading of the manuscript.

■ DEDICATION

†This paper is respectfully dedicated to the memory of our colleague and friend Professor Gian Piero Spada.

■ REFERENCES

(1) Kuhn, R. Molekulare Asymmetrie. In *Stereochemie*. Frendenberg, K., Ed.; Franz Deutike: Leipzig, Wien, 1933; p 803.
(2) (a) LaPlante, S. R.; Fader, L. D.; Fandrick, K. R.; Fandrick, D. R.; Hucke, O.; Kemper, R.; Miller, S. P. F.; Edwards, P. J. *J. Med. Chem.* **2011**, *54*, 7005−7022. (b) LaPlante, S. R.; Edwards, P. J.; Fader, L. D.; Jakalian, A.; Hucke, O. *Chem. Med. Chem* **2011**, *6*, 505−513.
(3) Bringmann, G.; Gulder, T.; Gulder, T. A. B.; Breuning, M. *Chem. Rev.* **2011**, *111*, 563−639.
(4) (a) Brunel, J. M. *Chem. Rev.* **2005**, *105*, 857−898. (b) Rueping, M.; Kuenkel, A.; Atodiresei, I. *Chem. Soc. Rev.* **2011**, *40*, 4539−4549.
(5) Mikami, K.; Aikawa, K.; Yusa, Y.; Jodry, J. J.; Yamanaka, M. *Synlett* **2002**, *10*, 1561−1578.
(6) Oki, M. *Top. Stereochem.* **1983**, *14*, 1−81.
(7) (a) Casarini, D.; Lunazzi, L.; Mazzanti, A. *Eur. J. Org. Chem.* **2010**, 2035−2056. (b) Bogdan, N.; Grosu, I.; Benoît, G.; Toupet, L.; Ramondenc, Y.; Condamine, E.; Dumitrescu, I. S.; Plé, G. *Org. Lett.* **2006**, *8*, 2619−2622.
(8) (a) Wolf, C. *Chem. Soc. Rev.* **2005**, *34*, 595−608. (b) D'Acquarica, I.; Gasparrini, F.; Pierini, M.; Villani, C.; Zappia, G. *J. Sep. Sci.* **2006**, *29*, 1508−1516. (c) Piron, F.; Vanthuyne, N.; Joulin, B.; Naubron, J.-V.; Cismaş, C.; Terec, A.; Varga, R. A.; Roussel, C.; Roncali, J.; Grosu, I. *J. Org. Chem.* **2009**, *74*, 9062−9070.
(9) Trapp, O.; Schoetz, G.; Schurig, V. *Chirality* **2001**, *13*, 403−414.
(10) (a) Coghlan, M. P.; Culbert, A. A.; Cross, D. A. E.; Corcoran, S. L.; Yates, J. W.; Pearce, N. J.; Rausch, O. L.; Murphy, G. J.; Carter, P. S.; Roxbee Cox, L. *Chem. Biol.* **2000**, *7*, 793−803. (b) Smith, D. G.; Buffet, M.; Fenwick, A. E.; Haigh, D.; Ife, R. J.; Saunders, M.; Slingsby, B. P.; Stacey, R.; Ward, R. W. *Bioorg. Med. Chem. Lett.* **2001**, *11*, 635−639. (c) Engler, T. A.; Malhotra, S.; Burkholder, T. P.; Henry, J. R.; Mendel, D.; Porter, W. J.; Furness, K.; Diefenbacher, C.; Marquart, A.; Reel, J. K. *Bioorg. Med. Chem. Lett.* **2005**, *15*, 899−903. (d) O'Neill, D. J.; Shen, L.; Prouty, C.; Conway, B. R.; Westover, L.; Xu, J. Z.; Zhang, H.-C.; Maryanoff, B. E.; Murray, W. V.; Demarest, K. T.; Kuo, G.-H. *Bioorg. Med. Chem.* **2004**, *12*, 3167−3185.
(11) Kaletas, B. K.; Mandl, C.; Van der Zwan, G.; Fanti, M.; Zerbetto, F.; De Cola, L.; König, B.; Williams, R. M. *J. Phys. Chem. A* **2005**, *109*, 6440−6449.
(12) Xie, H.; Ho, L. A.; Truelove, M. S.; Corry, B.; Stewart, S. G. *J. Fluoresc.* **2010**, *20*, 1077−1085.
(13) Barrett, S.; Bartlett, S.; Bolt, A.; Ironmonger, A.; Joce, C.; Nelson, A.; Woodhall, T. *Chem.—Eur. J.* **2005**, *11*, 6277−6285.
(14) (a) Casarini, D.; Lunazzi, L.; Mancinelli, M.; Mazzanti, A. *J. Org. Chem.* **2007**, *72*, 998−1004. (b) Lunazzi, L.; Mancinelli, M.; Mazzanti, A. *J. Org. Chem.* **2008**, *73*, 5354−5359.
(15) (a) Awuah, E.; Capretta, A. *J. Org. Chem.* **2011**, *76*, 3122−3130. (b) Dubernet, M.; Caubert, V.; Guillard, J.; Viaud-Massuard, M. C. *Tetrahedron* **2005**, *61*, 4585−4593. (c) Bouissane, L.; Sestelo, J. P.; Sarandeses, L. A. *Org. Lett.* **2009**, *11*, 1285−1288.
(16) (a) Mitchell, R. H.; Yan, J. S. H. *Can. J. Chem.* **1980**, *58*, 2584−2587. (b) Lunazzi, L.; Mazzanti, A.; Minzoni, M.; Anderson, J. E. *Org. Lett.* **2005**, *7*, 1291−1294. (c) Mazzanti, A.; Lunazzi, L.; Minzoni, M.; Anderson, J. E. *J. Org. Chem.* **2006**, *71*, 5474−5481.
(17) (a) Clough, R. L.; Roberts, J. D. *J. Am. Chem. Soc.* **1976**, *98*, 1018−1020. (b) Cozzi, F.; Cinquini, M.; Annunziata, R.; Siegel, J. S. *J. Am. Chem. Soc.* **1993**, *115*, 5330−5331. (c) Cozzi, F.; Ponzini, F.; Annunziata, R.; Cinquini, M.; Siegel, J. S. *Angew. Chem., Int. Ed. Engl.*

1995, *34*, 1019−1020. (d) Zoltewicz, J. A.; Maier, N. M.; Fabian, W. M .F. *Tetrahedron* **1996**, *52*, 8703−8706. (e) Zoltewicz, J. A.; Maier, N. M.; Fabian, W. M. F. *J. Org. Chem.* **1996**, *61*, 7018−7021. (f) Thirsk, C.; Hawkes, G. E.; Kroemer, R. T.; Liedl, K. R.; Loerting, T.; Nasser, R.; Pritchard, R. G.; Steele, M.; Warren, J. E.; Whiting, A. *J. Chem. Soc. Perkin Trans. 2* **2002**, 1510−1519. (g) Tumambac, G. E.; Wolf, C. *J. Org. Chem.* **2005**, *70*, 2930−2938.

(18) Lai, J.-H. *J. Chem. Soc., Perkin Trans. 2* **1986**, 1667−1670.

(19) (a) House, H.; Hrabie, J. A.; Van Derveer, D. *J. Org. Chem.* **1986**, *51*, 920−929. (b) House, H.; Holt, J. T.; Van Derveer, D. *J. Org. Chem.* **1993**, *58*, 7516−7523. (c) Lunazzi, L.; Mancinelli, M.; Mazzanti, A. *J. Org. Chem.* **2007**, *72*, 5391−5394.

(20) Cross, W.; Hawkes, G. E.; Kroemer, R. T.; Liedl, K. R.; Loerting, T.; Nasser, R.; Pritchard, R. G.; Steele, M.; Watkinson, M.; Whiting, A. *J. Chem. Soc., Perkin Trans. 2* **2001**, 459−467.

(21) Lai, Y.-H.; Chen, P. *J. Chem. Soc., Perkin Trans. 2* **1989**, 1665−1670.

(22) Lunazzi, L.; Mancinelli, M.; Mazzanti, A. *J. Org. Chem.* **2008**, *73*, 2198−2205.

(23) Gaussian 09, rev A.02: Frisch, M. J.; Trucks, G. W.; Schlegel, H. B.; Scuseria, G. E.; Robb, M. A.; Cheeseman, J. R.; Scalmani, G.; Barone, V.; Mennucci, B.; Petersson, G. A.; Nakatsuji, H.; Caricato, M.; Li, X.; Hratchian, H. P.; Izmaylov, A. F.; Bloino, J.; Zheng, G.; Sonnenberg, J. L.; Hada, M.; Ehara, M.; Toyota, K.; Fukuda, R.; Hasegawa, J.; Ishida, M.; Nakajima, T.; Honda, Y.; Kitao, O.; Nakai, H.; Vreven, T.; Montgomery, J. A., Jr.; Peralta, J. E.; Ogliaro, F.; Bearpark, M.; Heyd, J. J.; Brothers, E.; Kudin, K. N.; Staroverov, V. N.; Kobayashi, R.; Normand, J.; Raghavachari, K.; Rendell, A.; Burant, J. C.; Iyengar, S. S.; Tomasi, J.; Cossi, M.; Rega, N.; Millam, N. J.; Klene, M.; Knox, J. E.; Cross, J. B.; Bakken, V.; Adamo, C.; Jaramillo, J.; Gomperts, R.; Stratmann, R. E.; Yazyev, O.; Austin, A. J.; Cammi, R.; Pomelli, C.; Ochterski, J. W.; Martin, R. L.; Morokuma, K.; Zakrzewski, V. G.; Voth, G. A.; Salvador, P.; Dannenberg, J. J.; Dapprich, S.; Daniels, A. D.; Farkas, Ö.; Foresman, J. B.; Ortiz, J. V.; Cioslowski, J.; Fox, D. J. Gaussian, Inc., Wallingford, CT, 2009.

(24) (a) Jennings, W. B. *Chem. Rev.* **1975**, *75*, 307−322. (b) Mislow, K.; Raban, M. *Top. Stereochem.* **1967**, *1*, 1−38.

(25) Kruse, H.; Goerigk, L.; Grimme, S. *J. Org. Chem.* **2012**, *77*, 10824−10834.

(26) Taking into account the errors in the measurement of the sample temperature (±1 °C), also in this case the free energy was found to be invariant with the temperature, thus implying a negligible activation entropy.

(27) Lunazzi, L.; Mazzanti, A.; Muñoz Álvarez, A. *J. Org. Chem.* **2000**, *65*, 3200−3206.

(28) A solution of one atropisomer in hexane/2-propanol 90:10 was used to perform the kinetic study at 70 °C via HPLC analyses at regular times followed by first-order kinetic analysis.

(29) Peerdeman, A. F.; Van Bommel, A. J.; Bijvoet, J. M. *Nature* **1951**, *168*, 271−271.

(30) Hooft, R. W. W.; Stravera, L. H.; Spek, A. L. *J. Appl. Crystallogr.* **2008**, *41*, 96−103.

(31) For reviews, see: (a) Bringmann, G.; Bruhn, T.; Maksimenka, K.; Hemberger, Y. *Eur. J. Org. Chem.* **2009**, 2717−2727. (b) Crawford, T. D.; Tam, M. C.; Abrams, M. L. *J. Chem. Phys. A* **2007**, *111*, 12057−12068. (c) Pescitelli, G.; Di Bari, L.; Berova, N. *Chem. Soc. Rev.* **2011**, *40*, 4603−4625. (d) Mazzanti, D.; Casarini, D. *WIREs Comput. Mol. Sci.* **2012**, *2*, 613−641.

(32) MonteCarlo search with the MMFF force field, as implemented in TITAN 1.0.5, Wavefunction, Inc., Irvine, CA.

(33) In Gaussian 09 the BH&HLYP functional has the form: $0.5E_X^{HF} + 0.5E_X^{LSDA} + 0.5\Delta E_X^{Becke88} + E_C^{LYP}$.

(34) Zhao, Y.; Truhlar, D. G. *Theor. Chem. Acc.* **2008**, *120*, 215−241.

(35) Chai, J.-D.; Head-Gordon, M. *Phys. Chem. Chem. Phys.* **2008**, *10*, 6615−6620.

(36) Iikura, H.; Tsuneda, T.; Yanai, T.; Hirao, K. *J. Chem. Phys.* **2001**, *115*, 3540−3544.

(37) Yanai, T.; Tew, D.; Handy, N. *Chem. Phys. Lett.* **2004**, *393*, 51−57.

(38) (a) Cera, C.; Chiarucci, M.; Mazzanti, A.; Mancinelli, M.; Bandini, M. *Org. Lett.* **2012**, *14*, 1350−1353. (b) Pesciaioli, F.; Righi, P.; Mazzanti, A.; Bartoli, G.; Bencivenni, G. *Chem.—Eur. J.* **2011**, *17*, 2482−2485. (c) Duce, S.; Pesciaioli, F.; Gramigna, L.; Bernardi, L.; Mazzanti, A.; Ricci, A.; Bartoli, G.; Bencivenni, G. *Adv. Synth. Catal.* **2011**, *353*, 860−864. (d) Bernardi, L.; Comes-Franchini, M.; Fochi, M.; Leo, V.; Mazzanti, A.; Ricci, A. *Adv. Synth. Catal.* **2010**, *352*, 3399−3406.

(39) def2-TZVPP basis set coefficients for H,C,N,O were downloaded from the EMSL basis set exchange website: https://bse.pnl.gov/bse/portal. See: Weigend, F.; Ahlrichs, R. *Phys. Chem. Chem. Phys.*, **2005**, *7*, 3297−3305.

(40) Stephens, P. J.; McCann, D. M.; Devlin, F. J.; Cheeseman, J. R.; Frisch, M. J. *J. Am. Chem. Soc.* **2004**, *126*, 7514−7521.

(41) (a) Casarini, D.; Lunazzi, L.; Mancinelli, M.; Mazzanti, A.; Scafato, P. *Chirality* **2009**, *21*, 16−23. (b) Paradisi, E.; Righi, P.; Mazzanti, A.; Ranieri, S.; Bencivenni, G. *Chem. Commun.* **2012**, *48*, 11153−11260.

(42) Despite the fast interconversion rate, the transient-NOE technique gives valuable information about the ratio of the conformations because the observed enhancement is the result of the weighted sum of the NOEs of each conformation.

(43) Distances were calculated on the optimized structure as from: Claridge, T. D. W. *High-Resolution NMR Techniques in Organic Chemistry*, 2nd ed.; Elsevier: New York, 2009; pp 257−269.

(44) Absorption and CD data for such chromophore can be found in: Rosini, C.; Spada, G. P.; Proni, G.; Masiero, S.; Scamuzzi, S. *J. Am. Chem. Soc.* **1997**, *119*, 506−512. See also Berova, N.; Di Bari, L.; Pescitelli, G. *Chem. Soc. Rev.* **2007**, *36*, 914−931.

(45) Michl, J.; Thulsturp, E. W. *Spectroscopy with Polarized Light*; VCH Publishers: New York, 1986.

(46) Angiolini, L.; Benelli, T.; Giorgini, L. *Polymer* **2011**, *52*, 2747−2756.

(47) To get the best match with the experimental spectrum the simulated spectrum of the *anti*-out conformation was shifted by 6 nm with respect to that of the *anti*-in.

(48) An independent confirmation of this assignment could be derived from the simulation of a different chiro-optical spectrum such as VCD. Unfortunately, the calculated VCD spectra showed an opposite trend, and the experimental VCD spectrum of **4f** was very weak and prone to large simulation errors. The experimental spectra and the spectra simulated for the two conformations are reported in the Supporting Information.

(49) Because of the different priority in the definition of the dihedral angle between the naphthyl ring and the plane of maleimide, the *M* atropisomer of **3f** (the C-Br moiety has priority and defines the dihedral) has the same helicity of the *P,P* atropisomer of **4f** (C═O moiety has priority).

(50) Joyce, R. P.; Gainor, J. A.; Weinreb, S. M. *J. Org. Chem.* **1987**, *52*, 1177−1185.

(51) Prepared according to: Thompson, W. J.; Gaudino, J. *J. Org. Chem.* **1984**, *49*, 5237. See also: Pathak, R.; Nhlapo, J. M.; Govender, S.; Michael, J. P.; Van Otterlo, W. A. L.; De Koning, C. B. *Tetrahedron* **2006**, *62*, 2820−2830.

(52) Brown, J. H.; Bushweller, C. H. *DNMR6: Calculation of NMR Spectra Subject to the Effects of Chemical Exchange, (program 633)*; QCPE Bulletin: QCPE: Bloomington, IN, 1983; Vol. 3, pp 103−103. A copy of the program is available on request from the authors.

(53) Eyring, H. *Chem. Rev.* **1935**, *17*, 65−77.

(54) (a) Stonehouse, J.; Adell, P.; Keeler, J.; Shaka, A. J. *J. Am. Chem. Soc.* **1994**, *116*, 6037−6038. (b) Stott, K.; Stonehouse, J.; Keeler, J.; Hwang, T. L.; Shaka, A. J. *J. Am. Chem. Soc.* **1995**, *117*, 4199−4200. (c) Stott, K.; Keeler, J.; Van, Q. N.; Shaka, A. J. *J. Magn. Reson.* **1997**, *125*, 302−324. (d) Van, Q. N.; Smith, E. M.; Shaka, A. J. *J. Magn. Reson.* **1999**, *141*, 191−194.

(55) (a) Lee, C.; Yang, W.; Parr, R. G. *Phys. Rev. B* **1988**, *37*, 785−789. (b) Becke, A. D. *J. Chem. Phys.* **1993**, *98*, 5648−5652. (c) Stephens, P. J.; Devlin, F J.; Chabalowski, C. F.; Frisch, M. J. *J. Phys. Chem.* **1994**, *98*, 11623−11627.

(56) Package GaussView 5.0.9, Gaussian Inc., Wallingford CT, 2009.
(57) Ayala, P. Y.; Schlegel, H. B. *J. Chem. Phys.* **1998**, *108*, 2314−2325.
(58) (a) Wong, M. W. *Chem. Phys. Lett.* **1996**, *256*, 391−399. (b) Anconi, C. P. A.; Nascimiento, C. S., Jr.; Dos Santos, H. F.; De Almeida, W. B. *Chem. Phys. Lett.* **2006**, *418*, 459−466. (c) Wheeler, S. E.; McNeil, A. J.; Müller, P.; Swager, T. M.; Houk, K. *J. Am. Chem. Soc.* **2010**, *132*, 3304−3311.